

Styrene/Butadiene Gradient Block Copolymers: Molecular and Mesoscopic Structures

Stéphane Jouenne,^{†,‡} Juan A. González-León,[†] Anne-Valérie Ruzette,^{*,†}
Philippe Lodefier,[§] Sylvie Tencé-Girault,[†] and Ludwik Leibler[†]

Laboratoire Matière Molle et Chimie (UMR 7167 ESPCI–CNRS), ESPCI, 10 rue Vauquelin, 75005 Paris, France, and Total Petrochemicals, Pôle de Recherche et Développement de Mont, Lacq, France

Received November 27, 2006; Revised Manuscript Received January 17, 2007

ABSTRACT: Rubbery–glassy block copolymer dispersions are an attractive solution for toughening rigid thermoplastics like polystyrene without affecting optical transparency. An interesting facet of the copolymers used is molecular disorder, artificially introduced during anionic synthesis through composition gradients along the copolymer chain and/or blending and partial coupling of different copolymers. In particular, this level of disorder is apparently a key to achieve the desired PS/copolymer blend morphologies and properties in short processing times. In this work, we investigate the role of these “synthesis imperfections” on self-assembly of styrene-rich asymmetric gradient triblock copolymers, denoted S1–G–S2, where S_i are pure polystyrene blocks and G is a gradient copolymer of styrene and butadiene. Kinetic modeling of conversion data is used to predict gradient composition profiles for the anionic copolymerization conditions used. Self-assembly, dynamic viscoelastic behavior, and experimentally determined mesoscopic composition profiles across microdomains are discussed in light of the particular copolymer structure.

I. Introduction

Since the discovery of living anionic polymerization, scientific and technological interest in block copolymers as useful nanostructured plastics has kept increasing.^{1,2} Styrene/diene di- and triblock copolymers, such as SB or SBS, were among the first systems studied, and their triblocks are commonly used as thermoplastic elastomers, in adhesives and bitumen formulations, or as toughening additives. They are prepared by sequential additions and polymerization of separate styrene and diene monomer batches. The relevant architectural and molecular parameters that govern self-assembly and phase behavior are the overall degree of polymerization N , the respective length of each block, and the most probable microstructure of diene monomers under the synthesis conditions used. The phase behavior of these copolymers roughly follows theoretical predictions of model AB and ABA di- and triblocks,³ with a disordered state at high temperature and for low enough N . At lower temperature, the net repulsion between A and B forces stretching of the blocks in opposite directions and formation of separate A-rich and B-rich microdomains. This microphase separation transition,⁴ often referred to as the order/disorder transition or ODT, yields one of the following nanostructures depending on composition: lamellae for similar volume fractions of A and B, the double-gyroid over a narrow composition range adjacent to the lamellar phase, and hexagonally packed cylinders (Hex) or bcc spheres, for increasingly disparate volume fractions. Besides composition, molecular architecture and block sequence, as in multiblock, star, branched, or combed copolymers, further affects phase behavior and equilibrium morphologies.^{5–10} The most stable morphology is always dictated by a competition between conformational entropy changes and

contact energy minimization. The distance from the ODT is quantified by the degree of segregation χN , where χ is the dimensionless Flory–Huggins segmental interaction parameter scaling as $1/T$. At high values of χN , well-defined microdomains of almost pure A and pure B are separated by narrow interfaces. At intermediate and weak segregation strength, closer to the ODT, the interface becomes wider and composition profiles across microdomains are sinusoidal.

A second class of technologically important but less studied copolymers is gradient copolymers, also known as tapered block copolymers. These can be linear or star copolymers whose composition varies gradually along the chain from A-rich at one end to B-rich at the other end and can be described by a distribution function.¹¹ Gradient distributions spontaneously form in many living polymerization processes where two monomeric species with different reactivities are simultaneously introduced in a reactor. Such a “one pot” batch synthesis is fast and economic and therefore constitutes a large fraction of the block copolymer market in applications where an optimal balance between optical and mechanical properties is achieved for a minimum price. Although seldom quantified, the resulting molecular disorder along the copolymer chain is thought to be responsible for outstanding properties difficult to achieve in model sequential block copolymers.^{12–16}

Gradient copolymers have lately gained a lot of interest from polymer scientists.^{17,18} Theoretical models are starting to emerge that predict whether or not microphase separation can be expected and what type of morphology will form as a function of gradient composition distribution.^{19–21} These copolymers are less prone to microphase separation than analogous AB diblocks of similar N and global composition Φ_A and the disordered state occupies a large area of the phase diagram. Self-assembled morphologies are predicted for certain monomer distribution functions and segregation strengths. The nature, size, and periodicity of microdomains are strongly influenced by this distribution, and so is the coexistence curve. In particular, linear composition profiles are predicted to only yield the lamellar

* To whom correspondence should be addressed.

[†] Laboratoire Matière Molle et Chimie (UMR 7167 ESPCI–CNRS), ESPCI.

[‡] Current address: Total Petrochemicals, Pôle de Recherche et Développement de Mont, Lacq, France.

[§] Total Petrochemicals, Pôle de Recherche et Développement de Mont.

phase independent of overall composition and for extreme levels of segregation, while other morphologies are possible for continuous but nonlinear distribution functions.¹⁹ Sinusoidal composition profiles across microdomains as well as broad interfaces reminiscent of weakly segregated block copolymers are always predicted even at high segregation strength.²¹

Kraus et al.^{22,23} first prepared model SB gradient copolymers by a one-pot anionic synthesis in cyclohexane and reported their visco-elastic behavior. Shortly after, Tsukahara et al.^{15,24} and Gronski and co-workers²⁵ reported the self-assembly and dynamic rheological behavior of similar SI^{24,25} and SB²⁴ linear gradient or gradient-block copolymers of various architectures. Neat gradient copolymers were found to display a single yet broad glass transition temperature T_g despite microdomain formation. In contrast, gradient/block copolymers with a gradient sequence linked to a more or less pure second block always displayed two T_g 's. The weak contrast of TEM micrographs for stained gradient copolymers was attributed to substantial mixing of monomers within microdomains. This was confirmed by small-angle X-ray scattering (SAXS)²⁴ and modeling of the dynamic mechanical response as a function of temperature.^{24,25} These studies also suggested that inserting a gradient section between pure S and B blocks is a very efficient way to modify interfacial width and potentially mechanical properties of block copolymers. Gradient/block copolymers of the A–A/B–B type have indeed received special attention.^{26–29} The gradient or statistical middle block decreases domain spacing and incompatibility, and increases interfacial width considerably. More recently, in a seminal series of papers recently reviewed by the authors,³⁰ Michler and co-workers studied self-assembly and tensile properties of SBS triblock and (SB)_n star copolymers of various chemical structures, often with gradient or statistical soft blocks and asymmetric S blocks. The exact composition profiles and molecular architecture of copolymers with gradient sections were not known, which makes interpretation of some results delicate. Still, a striking observation has been made that, at fixed N and total Φ_S , gradient middle blocks strongly shift copolymer morphologies. Hence, the authors reported lamellar phases at only 26 wt % B for linear³¹ and star³² gradient block copolymers with asymmetric S blocks. This change in morphology was accompanied by large changes in tensile behavior compared with architecturally symmetric block copolymers of same N and composition.³⁰ But the effect of a gradient section was not explicitly separated from that of the complex architectural asymmetry.

In this work, we further elucidate the role of gradient sections in linear gradient triblock copolymers of the S1–G–S2 type, where S1 and S2 are short and long styrene blocks, respectively, and G is a gradient copolymer of S and B evolving from B-rich to S-rich along the chain. These copolymers are prepared by a two step anionic synthesis: after a first homopolymerization S1, a second copolymerization step yields the gradient and final block S2. Ideally, one should be able to specifically tailor properties of such gradient block copolymer by slight modifications of synthesis conditions. The chemical kinetics leading to this kind of copolymers is indeed understood^{33,34} and can be modeled provided reactivity ratios r_i between different monomer species are known. Unfortunately, this is seldom the case as they vary with synthesis conditions. Here, the Markov (terminal) model is used to describe experimental conversion data over time for the copolymerization step and determine the shape of the gradient composition profile under the synthesis conditions used. Exact molecular structure and the resulting triblock architectural asymmetry are also quantified. Near equilibrium

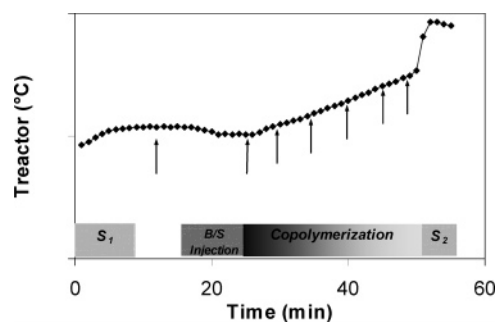


Figure 1. Evolution of reactor temperature for the two step adiabatic synthesis of S1–G–S2. Arrows indicate times where aliquots were taken just before and during the copolymerization (second) step.

and dynamic (under strong shear) self-assembly of these gradient copolymers is explained in light of their structure. An asymmetric triblock with a pure B middle block, S1–B–S2, is also studied to separate the role of the gradient middle block from that of architectural asymmetry. Modeling microdomain periods determined by SAXS is used to elucidate possible block arrangements in these asymmetric triblocks. A simple method based on the Kerner composite equation³⁵ combined with the Gordon Taylor expression³⁶ is further proposed to extract mesoscopic composition profiles across microdomains from dynamic mechanical data. These illustrate well the effect of the gradient middle block on self-assembly. The link between these profiles and tensile behavior of these copolymers and their nanostructured blends with polystyrene will be presented in a companion paper.

II. Experimental Section

The S1–G–S2 gradient block copolymers studied here were prepared by a two step living anionic synthesis in cyclohexane in a laboratory-scale adiabatic reactor. Monomers and solvents were purified on activated alumina columns to remove stabilizing agents and polar moieties. Cyclohexane mixed with 50–150 ppm of tetrahydrofuran (THF) was loaded first in a double-jacket stainless-steel reactor equipped with a mechanical stirring arm. The reactor was brought to the starting temperature T_{init} and a first batch of styrene monomers was added under nitrogen. The desired amount of initiator (*sec*-butyllithium, *s*BuLi) was incorporated with a dry and clean glass syringe and polymerization of S1 blocks started to proceed. This homopolymerization is accompanied by a temperature rise which stabilizes after 10 min once all styrene monomers have been consumed, as indicated by a first plateau on the typical reactor temperature plot shown in Figure 1. A first aliquot was then taken to characterize the S1 block, and a mixed batch of cold styrene and butadiene monomers was added for the copolymerization (second) step. Under the synthesis conditions used here, butadiene reacts first along with a few styrene units incorporated in a statistical fashion. Temperature rises linearly and aliquots, indicated by arrows on the T profile of Figure 1, were taken at fixed time intervals to follow conversion and the evolution of copolymer composition. Once all B monomers have reacted, a sudden temperature rise indicates homopolymerization of the terminal block S2. Several syntheses were performed, all at a fixed composition, but with varying amounts of THF. Two will be discussed here. Aliquots extracted from the reactor were terminated by a phenol derivative. The solutions were used as is for SEC analysis and absolute molecular weights were determined based on an existing calibration for high molecular weight S-rich SB copolymers.³⁷ For ¹H NMR, aliquots were precipitated in methanol, dried and dissolved in deuterated chloroform (CDCl₃). This technique not only yields the global fraction of styrene F_S (in mol %) that has been incorporated in the copolymer over time, but also how much of these styrene units were incorporated in a statistical fashion. Indeed, H atoms in *ortho* position on the benzene ring of S units adjacent to another S

unit present a distinct chemical shift from protons on the *meta* and *para* position.³⁸ This is not the case for BSB triads and their fraction, referred to as the statistical styrene fraction $F_{S,stat}$ is easily deduced. Proton NMR also gives the butadiene microstructure, namely the ratio of 1,2- to 1,4-butadiene units, which lies around 0.15 for all copolymers. Unfortunately, the monomer mixture composition was not directly accessible from NMR. For low number-average molecular weights M_n , the SEC calibration used is also not sufficiently accurate to follow conversion. Here, conversion was instead estimated from the fraction of statistical styrene units determined by NMR, as will be explained in section III.1.

Two purely blocky analogues of the gradient copolymers described above, with same overall N and styrene volume fraction Φ_S , were also studied. The first one is an asymmetric triblock S1–B–S2 with a pure B middle block and prepared in three steps: a first homopolymerization of S1, a second homopolymerization of all B monomers, and a third homopolymerization of a correspondingly longer S2. This copolymer will help separate the effect of a gradient middle block from the asymmetry between S1 and S2. The symmetric analogue of this copolymer, denoted S–B–S, with the same B middle block but outer S blocks of equal length, was graciously supplied by Total Petrochemicals. Two polystyrene homopolymers of controlled molecular weights and polydispersity were also prepared by bulk radical polymerization controlled with the nitroxide *N-tert-butyl-N-(1-diethylphosphono-2,2-dimethylpropyl)-N-oxyl*, denoted DEPN.³⁹ The synthesis protocol was identical to that described elsewhere for butyl acrylate (BA) homopolymers and acrylic copolymers.⁴⁰ A long PS sample of $M_n = 110$ kg/mol and polydispersity index PDI = 1.37 was used as a reference for dynamic mechanical analysis and modeling of copolymer moduli with temperature. A short PS (PS22, $M_n = 22$ kg/mol, PDI = 1.24) was also prepared, to be used in blends with copolymers and probe robustness of their equilibrium morphologies.

Combined TEM and SAXS were used to investigate bulk self-assembled morphologies of the copolymers both under static conditions close to thermodynamic equilibrium and after extrusion in a laboratory-scale microcompounder. Solvent cast films, ca. 300 μm thick, were obtained by slow evaporation (over 2 weeks) of 5 wt % solutions of copolymers in toluene. The obtained films were dried under vacuum at 60 °C and annealed for 2 days at 180 °C. To prevent thermal degradation, samples were allowed to cool slowly to 100 °C before breaking the vacuum. Copolymer melt extrusion was performed at 180 °C on a 5 cm³ capacity DACA twin-screw microcompounder equipped with a recirculation valve. Three grams of copolymer were introduced in the closed microcompounder and sheared for 3 min at a screw rotating speed of 60 rpm. The recirculation valve was then opened and the copolymer melt was extruded through a cylindrical die with a diameter of 1.85 mm.

Transmission electron microscopy (TEM) was performed on ultrathin sections, ca. 50 nm thick, cut with a diamond knife at –100 °C on a Leica Ultracut cryo-microtome. Sections were collected on 400 mesh copper grids and exposed to Osmium tetroxide (OsO₄) vapors for 45 min. Transmission electron micrographs were obtained on a JEOL 100CX TEM operated at 100 kV. For extruded samples, sections were cut both perpendicular and parallel to the extrusion direction.

SAXS was performed at room-temperature using a Cu K α radiation. Solvent cast films were tested as is, while extruded strands were first pressed at 170 °C on a Carver hydraulic press to obtain ca. 0.3 mm-thick films. Transmitted scattered intensity was collected on a LPS55 linear detector from INEL. The sample–detector distance was 1.3 m, resulting in a q range from 0.008 to 0.09 \AA^{-1} . A volume of ~ 0.4 mm³ was sampled by the beam and isotropy at this scale was verified. Scattered intensity was corrected for blank background scattering and will be given in arbitrary units as a function of wave vector $q = (4\pi/\lambda) \sin \theta$, where θ is half the scattering angle and λ is the wave length of 1.54 \AA .

The stability of the ordered state even up to high temperatures used for melt processing was verified by dynamic rheological testing

on all copolymers using a Rheometric Scientific ARES rheometer. Copolymer disks melt pressed at 170 °C were placed between parallel plates 25 mm in diameter separated by a 0.5 mm gap. Copolymers were subjected to a 1% in amplitude oscillatory shear deformation which was verified to lie in the linear regime. Dynamic storage (G') and loss (G'') moduli were determined isothermally as a function of frequency ($0.1 < \omega < 100$ rad/s), and temperature was varied from 150 to 250 °C in 10 °C increments. Linear viscoelastic behavior of the copolymers was also recorded at lower temperatures up to the glass transition of polystyrene on a DMA 2980 Dynamic Mechanical Analyzer from TA Instruments. Rectangular bars, $L \times l = 20$ mm \times 5 mm, were machined out of solvent cast or extruded and pressed films and placed in a sample holder operated in tension. They were cooled to –125 °C and subjected to a 0.1% in amplitude sinusoidal tensile deformation at a frequency of 1 Hz. The evolution of storage (E') and loss (E'') Young moduli was recorded upon heating to 150 °C at 2 °C/min. T_g 's of the microphases were taken at the maxima of $\tan \delta$ given by the ratio of loss to storage modulus, where δ is the phase lag between the imposed oscillatory deformation and the dynamic response of the material.

III. Results and Discussion

III.1. Gradient Composition Profile. Anionic copolymerization of S and B in nonpolar hydrocarbon solvents such as cyclohexane or benzene yields a strong composition gradient since $r_S = k_{SS}/k_{SB}$ is much smaller than $r_B = k_{BB}/k_{BS}$, where k_{ii} are the usual homo- and cross-propagation reaction constants.^{41–43} A competition is thus set between monomer reactivity and concentration, and chains evolve from B-rich to S-rich with conversion. In polar solvents and at low temperature, the opposite holds, and S can be more reactive than B. For this system, it is thus possible to tune monomer reactivity and the resulting copolymer composition profile by playing with monomer mixture composition, reaction temperature and the ratio of nonpolar to polar species.^{41,42,44–46}

The simplest kinetic model taking cross-propagation effects into account is the first order Markov terminal model.³⁴ It assumes that reactivity of a growing chain is only a function of the last monomer unit incorporated. Here, we further consider that propagation reactions are irreversible and that the growing chains are living due to the absence of chain transfer and chain termination reactions. Finally, initiation is much faster than propagation and the assumption of high molar mass copolymer molecules is sufficient. Under these conditions, integrating a mass balance for each monomer type yields the following relation between molar conversion p , and the molar fractions x_S and $x_B (= 1 - x_S)$ in the reacting monomer mixture:⁴⁷

$$p = 1 - \frac{[M]}{[M]^0} = 1 - \left[\frac{x_B}{x_B^0} \right]^a \left[\frac{x_S}{x_S^0} \right]^b \left[\frac{x_B^0 - x^*}{x_B - x^*} \right]^c \quad (1)$$

where $[M]$ and $[M]^0$ are the current and initial (total) monomer concentrations (in mol/L), a , b , c and x^* are functions of r_S and r_B given by eq 2 and x_S^0 et x_B^0 are initial fractions of S and B in the comonomer feed.

$$a = \frac{r_S}{(1 - r_S)}, \quad b = \frac{r_B}{(1 - r_B)}, \quad c = \frac{(1 - r_S r_B)}{(1 - r_S)(1 - r_B)}, \quad x^* = \frac{(1 - r_S)}{(2 - r_S - r_B)} \quad (2)$$

Likewise, the average styrene fraction f_S of the growing copolymer chains is given by

$$f_S = \frac{x_S^0 - (1-p)x_S}{p} \quad (3)$$

while the instantaneous, or local, styrene fraction at conversion p is given by the copolymerization equation:^{33,34}

$$f_{S,\text{inst}} = f_S + p \frac{\partial f_S}{\partial p} = \frac{x_S(r_S x_S + x_B)}{r_S x_S^2 + 2x_S x_B + r_B x_B^2} \quad (4)$$

This fraction gives the probability of having an S or B monomer at each position along the chain, and thus the gradient composition profile. Equations 1–4 indicate that r_S , r_B and the initial monomer feed composition completely determine the final shape of this profile. Experimental determination of x_S and p for a given synthesis can be used to determine reactivity ratios using eq 1. This information was not directly accessible experimentally but could be inferred from ¹H NMR data on aliquots using the measured fraction of statistical styrene units, $F_{S,\text{stat}}$ (the mole fraction of BSB triads for the whole copolymer chain). On the basis of previous S/B copolymerization studies performed under similar conditions, it can indeed be assumed that all S monomers incorporated in the first stages of the copolymerization step are statistical. In pure cyclohexane and for similar monomer feed compositions, nonstatistical styrene units only start to appear at 50% conversion.⁴³ In this case, we can write at lower conversions of the copolymerization step:

$$\frac{F_{S,\text{stat}}}{F_S} = \frac{n_{S,B/S}}{n_{S,B/S} + n_{S1}} \quad (5)$$

where F_S and $F_{S,\text{stat}}$ are the total fractions of styrene and statistical styrene units accessible from NMR, which take into account the gradient second block as well as the first block S1. The number of moles of S incorporated during S1 homopolymerization, n_{S1} , is known, and the number of moles of styrene reacted at time t of the copolymerization step, denoted $n_{S,B/S}$, is thus easily determined from eq 5. Likewise, $n_{B,B/S}$, the amount of B monomers reacted at time t , is readily available:

$$n_{B,B/S} = \frac{F_B}{F_S} \times (n_{S,B/S} + n_{S1}) \quad (6)$$

Monomer conversion, free monomer mixture composition, and average copolymer composition, now defined for the copolymerization step of the synthesis only, are then given by

$$p = \frac{n_{S,B/S} + n_{B,B/S}}{n_{S,B/S}^0 + n_{B,B/S}^0}, x_S = \frac{n_{S,B/S}^0 - n_{S,B/S}}{n_{B/S}^0 - n_{B/S}}, f_S = \frac{n_{S,B/S}}{n_{S,B/S} + n_{B,B/S}} \quad (7)$$

where $n_{S,B/S}^0$, $n_{B,B/S}^0$, and $n_{B/S}^0$ are the styrene, butadiene and total number of moles initially present in the comonomer feed and $n_{B/S} = n_{S,B/S} + n_{B,B/S}$. Figure 2 gives a typical evolution of f_S and x_S with conversion for the copolymerizations performed here. These data points can be fit with eqs 1–3 up to maximum conversions of 50% to extract average reactivity ratios. A least-square fitting procedure yields $r_S = 0.04$ and $r_B = 8.88$ for the particular case illustrated in Figure 2a. In pure cyclohexane, Johnson et al. determined r_S and r_B values of 0.04 and 26, respectively.⁴³ The average values determined here are compatible with these results as well as the expected role of THF, known to decrease r_B/r_S . Note, however, that reactivity ratios are a function of temperature, which is not fixed under the adiabatic reaction conditions of the present syntheses. The

extracted average values are thus not directly applicable to other monomer feed compositions. Yet they can be used to calculate the instantaneous copolymer composition for this particular synthesis using eq 4. The results are shown in Figure 2b where $f_{S,\text{inst}}$ is plotted along with f_S , $f_{S,\text{stat}}$, and $f_{S,\text{bl}}$. The latter is the fraction of SSS, SSB and BSS triads and is given by $f_S - f_{S,\text{stat}}$. The fraction of statistical styrene is obtained by integrating the probability product $p_{BS} \cdot p_{SB}$, where $p_{BS} = (x_S)/(r_B x_B + x_S)$ is the probability of forming a BS dyad and $p_{SB} = (x_B)/(r_S x_S + x_B)$ is the probability of forming an SB dyad:

$$f_{S,r} = \frac{1}{p} \int_{p=0}^p (p_{BS} \times p_{SB}) dp \quad (8)$$

The profiles of Figure 2b give the exact molecular structure of the gradient copolymer: initially rich in B (~90 mol %), it slowly and then abruptly evolves toward the pure block S2. The profiles of Figure 2b also validate the hypothesis that all styrene is originally added under the form of BSB triads during copolymerization. Other triads, given by $f_{S,\text{bl}}$, only form above 55% conversion. At about 67% conversion, 99.9% B has reacted and this is defined as the beginning of the pure block S2. The resulting block length $M_{n,S2}$ is reported in Table 1 for two different syntheses, along with the final copolymer molecular weight and PS end block asymmetry $\tau = (S1)/(S1 + S2)$. The global styrene and statistical styrene fractions listed in Table 1 are those determined by ¹H NMR and include S1. The characteristics of the two nongradient symmetric (S–B–S) and asymmetric (S1–B–S2) triblocks are also given.

III.2. Near-Equilibrium Self-Assembly. Solvent cast and annealed films of the copolymers listed in Table 1 were all transparent and nanostructured. Typical morphologies observed by TEM are shown in Figure 3 for S1–G–S2, S1–B–S2, and S–B–S stained with OsO4. B-rich microdomains thus appear dark while S microdomains are light. As expected based on its composition and molecular weight, S–B–S forms cylindrical B microdomains hexagonally packed in an S matrix (Figure 3c). This observation is confirmed by the SAXS intensity profile obtained on the same film at room temperature and shown under the corresponding TEM micrograph (Figure 3f). Diffraction peaks at indicated multiples of q^* are compatible with hexagonal order. The distance between cylinder layers $D = 2\pi/q^*$ is reported in Table 2. The average distance between cylinders is $d = (2/\sqrt{3})D = 37\text{nm}$. Note that all copolymer samples were treated as isotropic distributions of structured grains and peak positions q^* reported in Table 2 were thus determined after applying the Lorentz correction.

S–B–S is the only copolymer presenting an interface curved toward B, the minority component. Despite their majority of styrene, S1–G–S2, S1–G–S2b (data not shown), and S1–B–S2 adopt a lamellar morphology, as evidenced by the TEM micrographs (a and b) and corresponding scattering profiles (d and e) displaying peaks at integer multiples of q^* . Peak positions obtained after the Lorentz correction and corresponding lamellar spacings are listed in Table 2. These roughly coincide with those measured on TEM micrographs. Since the two gradient copolymers S1–G–S2 and S1–G–S2b displayed very similar behavior, only the first one will be further discussed.

Based on composition, a lamellar morphology with flat interfaces for S1–G–S2 and S1–B–S2 is surprising at first. Similar results were reported by Michler and co-workers for star and linear SBS gradient block copolymers.^{31,32} Asymmetry of the outer styrene blocks ($S1 < S2$) is partially responsible for it and its importance can be quantified. Asymmetric triblock copolymers (without gradient) have indeed been treated theo-

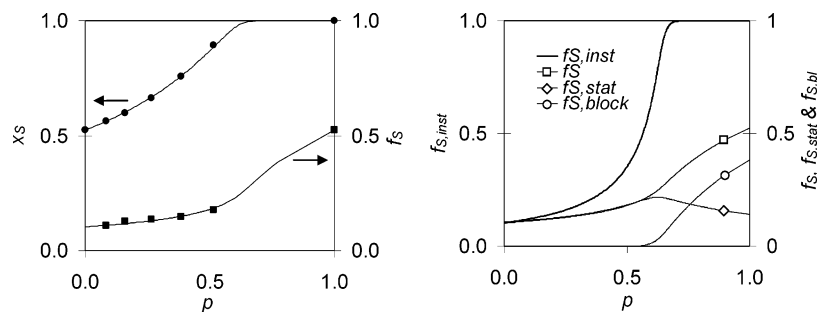


Figure 2. (a) Average copolymer composition f_S and free monomer mixture composition x_S as a function of conversion p for the copolymerization step of S1–G–S2. Symbols indicate experimental data points while the full curves are least-square fits using r_S and r_B values of 0.04 and 8.88, respectively. (b) Gradient composition profile given by the evolution of the instantaneous molar fraction of styrene $f_{S,inst}$ with conversion (left axis). The right axis gives the average styrene fraction (f_S), the fraction of BSB triads $f_{S,stat}$, and the fraction of block styrene $f_{S,bl}$. All concentrations refer to the copolymerization step only and do not take into account the first block S1.

Table 1. Molecular Structure of Gradient and Nongradient Triblock Copolymers

	F_S^a	$F_{S,stat}^a$	Φ_S^b	M_n^c	PDI	$M_{n,S2}$	τ
S1–G–S2	0.58	0.11	0.71	121	1.04	46	0.25
S1–G–S2b	0.59	0.13	0.72	116	1.04	42	0.25
S1–B–S2	0.58	0	0.71	112	1.08	70	0.15
S–B–S	0.62	0	0.74	130	1.34	50	0.50

^a Total molar fractions of S units and BSB triads determined by ¹H NMR (these include S1). ^b Overall styrene volume fraction calculated with mass densities for PS and PB of 1.05 and 0.95 g/cm³, respectively. ^c Molecular weights are in kg/mol and were determined by SEC using an internal calibration, or were calculated ($M_{n,S2}$) from the gradient composition profiles determined in section III.1

retically.^{6,10} For an asymmetry $\tau = 0.15$ and a segregation strength $\chi N = 40$, self-consistent field calculations predict a shift of the stability domain of the lamellar phase toward higher fractions of the outer blocks Φ_A . Lamellae can form up to $\Phi_A = 73$ vol %, against 65 vol % for symmetric triblocks or equivalent diblocks. The segregation strength of S1–B–S2 can be calculated using the interaction parameter $\chi_{SB} = 6.59 \times 10^{-3} + 13.6/T$ determined by Sakurai et al.⁴⁸ and lies around 57 at 373 K, the T_g of PS below which morphologies are frozen upon slow cooling. Since the effect of asymmetry is predicted to increase with segregation strength,¹⁰ a lamellar morphology can be explained for S1–B–S2.

For S1–G–S2, the presence of a gradient middle block should decrease segregation strength. A first and very rough approximation of this decrease can be obtained by treating the gradient middle block G as a statistical block containing $x_{S,G} = (F_S N - N_{S1} - N_{S2}) / (N - N_{S1} - N_{S2})$ styrene units, where N_{S1} and N_{S2} are the degrees of polymerization of pure S blocks and N is the total degree of polymerization given in Table 2. A Flory-type analysis predicts an effective interaction parameter χ_{eff} between this statistical block and pure styrene blocks given by⁴⁹

$$\chi_{eff} = (1 - x_{S,G})^2 \chi_{SB} \quad (9)$$

The resulting segregation strength of S1–G–S2 at 373 K is given in Table 2. Besides its lower χ , asymmetry is also less pronounced for S1–G–S2 (higher τ) since S2 is shorter. At 70 vol % S, theory predicts a cylindrical phase. However, the volume fraction of styrene outer blocks to be considered here is considerably lower than Φ_S , a lot of styrene units being statistically incorporated in the gradient middle block. Let us assume that only pure styrene blocks constitute the white (hard) lamellar microdomains of these gradient triblock copolymers (dynamic mechanical data, presented in section III.4, indeed indicates that all copolymers comprise pure PS microdomains). The correct composition to be considered is thus $\Phi_{S1+S2} \sim 50\%$,

and not $\Phi_S = 70\%$. Under these conditions ($\chi N \sim 26$, $\tau = 0.25$ and 50 vol % outer blocks), theory also predicts a lamellar morphology.¹⁰

It is important to further elucidate the most plausible arrangement of individual blocks (S1, S2, G, or B) within the lamellar phases of these asymmetric triblocks. This will have important consequences on the mechanical properties, to be discussed in a companion paper. One possibility is that S1, if short enough, is partially dragged into B-rich microdomains. This can occur for a critical asymmetry and, in the extreme case of very short S1, the asymmetric triblock can even behave as an equivalent diblock,¹⁰ here (S1–B)–S2 or (S1–G)–S2. The lamellar period of these pseudo-diblocks can be calculated according to⁵⁰

$$D_{AB} = \frac{4}{\sqrt{6}} \left(\frac{3}{\pi^2} \right)^{1/3} a N^{2/3} \chi^{1/6} \quad (10)$$

where a is an average statistical segment length defined as the geometric mean of $a_S = 0.67$ nm and $a_B = 0.63$ nm⁵¹ and N is the total number of segments. The appropriate χ parameter between (S1–B) or (S1–G) and S2 blocks is computed according to eq 9, where x_S is the fraction of styrene units in these pseudo-first blocks. This yields a lamellar period D_{AB} of 45 to 50 nm, much higher than the SAXS-based lamellar periods reported in Table 2. This block arrangement with S1 blocks mixed into B microdomains is thus not compatible with experiments. Instead, S1 blocks will more likely self-assemble in a bidisperse brush with S2 blocks. The molecular origin of the lamellar phases observed is then essentially similar to the co-surfactant effect in binary blends of diblock copolymers with short and long A blocks.^{52–55} In fact, it is interesting to treat the asymmetric triblocks as such binary blends of long (l) and short (s) diblocks obtained by cutting the triblock chain at the center of its middle block. The lamellar period of such binary blend has been adapted from Birshtein et al.⁵² by Court and Hashimoto and can be calculated according to⁵⁵

$$D_{ls} = \frac{4}{\sqrt{6}} \left(\frac{3}{\pi} \right)^{1/3} a \bar{N}^{2/3} \chi^{1/6} f(n_l)^{-1/3} \quad (11)$$

where

$$f(n_l) = (1 + n_l^3(N_l/N_s - 1))(1 + n_l(N_l/N_s - 1))^{-1} \quad (12)$$

In our case, the proportion of long chains $n_l = 0.5$ and the average chain length is $\bar{N} = (N_l + N_s)/2$ where $N_l = 1/2(N + N_{S2} - N_{S1})$ and $N_s = 1/2(N + N_{S1} - N_{S2})$ are readily calculated from the data given in Table 1. The statistical segment length

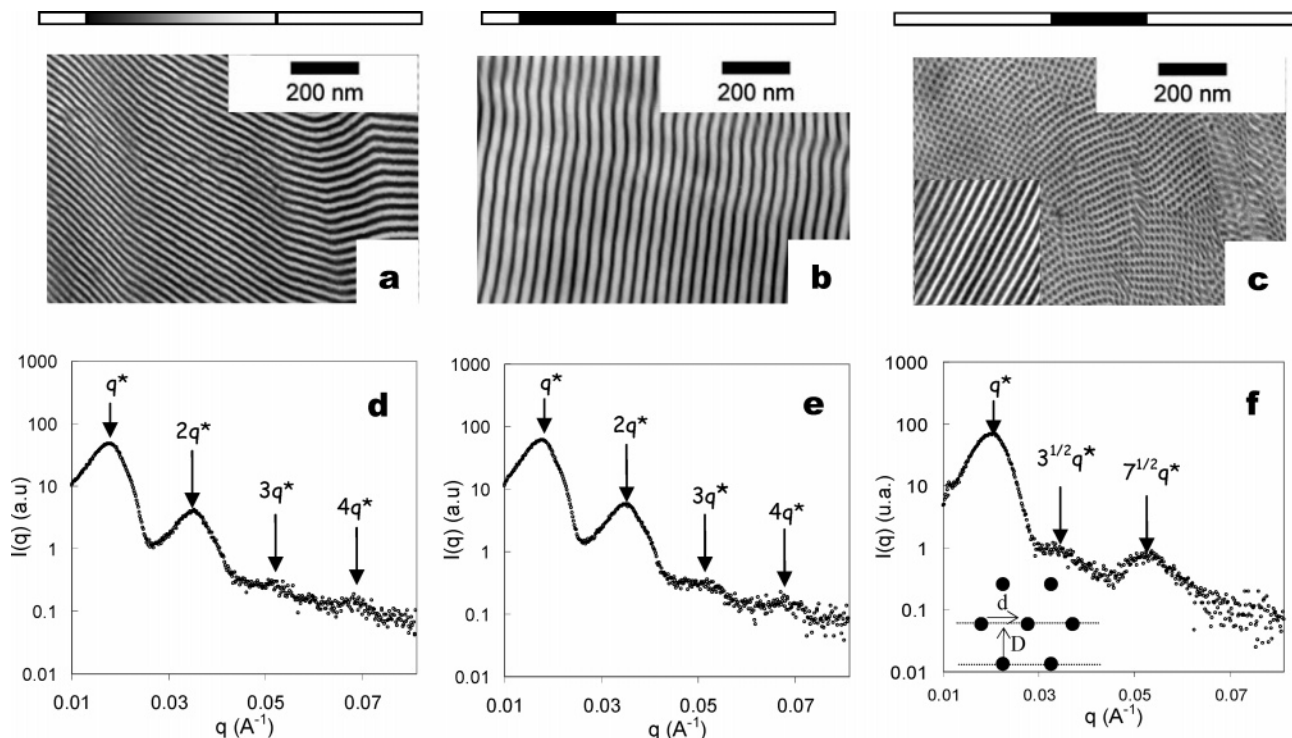


Figure 3. TEM micrographs (a–c) and room-temperature SAXS profiles (d–f) of solvent cast and annealed films of S1–G–S2 (a, d), S1–B–S2 (b, e) and S–B–S (c, f) with molecular structures schematically represented on top of the micrographs.

Table 2. Experimental and Theoretical Interdomain Distances

	morphology	q^* (\AA^{-1})	D_{SAXS}^a (nm)	$\chi_{\text{eff}}^* N^b$	D_{AB}^c (nm)	D_{is}^d (nm)	N	τ
S1–G–S2	lam	0.0175	36	29	46	32	1447	0.25
S1–G–S2b	lam	0.0182	34.5	26	44	31	1388	0.25
S1–B–S2	lam	0.0173	36	57	49	37	1350	0.15
S–B–S	cyl	0.0197	32	65			1533	0.50

^a Interdomain spacing $2\pi/q^*$ corresponding to the lamellar period or the distance between planes of cylinders. ^b Segregation strength at 373 K ($T_{\text{g,ps}}$) with $\chi_{\text{SB}} = 6.59 \times 10^{-3} + 13.6/T$. ^c Theoretical lamellar periods of equivalent diblocks where S1 mixes with G or B. ^d Theoretical lamellar periods of binary blends of l (long) and s (short) diblocks obtained by cutting S1–G–S2 or S1–B–S2 at the center of the middle block.

a is the same as above. The thus calculated periodicities are given in Table 2 for each lamellar copolymer. They are in much better agreement with SAXS data, confirming that S1 and S2 blocks self-assemble within the same microdomains. Short blocks are expected to localize close to the interface and long ones at the center, and this is precisely the co-surfactant effect that flattens the interface despite a majority of styrene blocks. From a mechanical standpoint, this block arrangement is essential since it allows bridging configurations of the copolymer chains and far superior mechanical resistance compared to diblocks. This fixes limitations on how short S1 can be.

To then discriminate between S1–G–S2 and S1–B–S2 and further elucidate the role of the gradient section on near-equilibrium self-assembly, small amounts of short polystyrene homopolymer chains were blended with these triblocks. To this end, 85 wt % triblock was co-dissolved with 15 wt % PS22 ($M_n = 22$ kg/mol, PDI = 1.24) in toluene (5 wt % solution). Transparent films of these blends were cast and annealed as described for pure copolymers. Figure 4 shows micrographs of two blends of S1–G–S2 (left) and S1–B–S2 (right) with 15 wt % PS22. The right micrograph reveals a perforated lamellar morphology for S1–B–S2 swollen with PS chains. This morphology has been observed between the lamellar and gyroid phases of diblocks⁵⁶ and blends⁵⁷ and is believed to be metastable. Here, it suggests that neat S1–B–S2 is not far from the lamellar/cylinder stability border, as predicted by SCF calculations.¹⁰ In contrast, the left micrograph of Figure 4 reveals

a lamellar morphology for S1–G–S2 despite the addition of 15 wt % PS. The robustness of this lamellar phase, already reported by Adhikari et al. for similar triblocks with random instead of gradient middle blocks,⁵⁸ is consistent with the stiffening effect of gradient or statistical interfaces in $A-(A/B)_s-B$ block copolymers.²⁸ The effective volume fraction of pure styrene blocks (S1 + S2) of only 50% for S1–G–S2 also explains the increased stability of its lamellar phase.

III.3. Gradient Copolymers Self-Assembly under Shear.

The morphologies presented above formed under conditions as close as possible to thermodynamic equilibrium, i.e., very slow solvent evaporation from a dilute solution followed by prolonged annealing in the molten state and subsequent slow cooling. It is important to specify that all copolymers remained microphase separated throughout this process, since no ODT could be detected by dynamic rheological testing up to 250 °C. For example, data for S1–G–S2, not shown here, indicated a low-frequency power law behavior of G' and G'' scaling as $\omega^{0.5}$ at all temperatures. At 180 °C, the temperature of annealing and melt processing, all copolymers are thus expected to be microphase separated.

Morphologies are strongly affected by the complex flow fields developed in laboratory-scale microcompounders that mimic large-scale extruders. After 3 min of melt-mixing at 180 °C followed by extrusion through the exit die, all copolymers present ill-defined microphase separated morphologies lacking long-range order. This is illustrated in Figure 5. Left micrographs

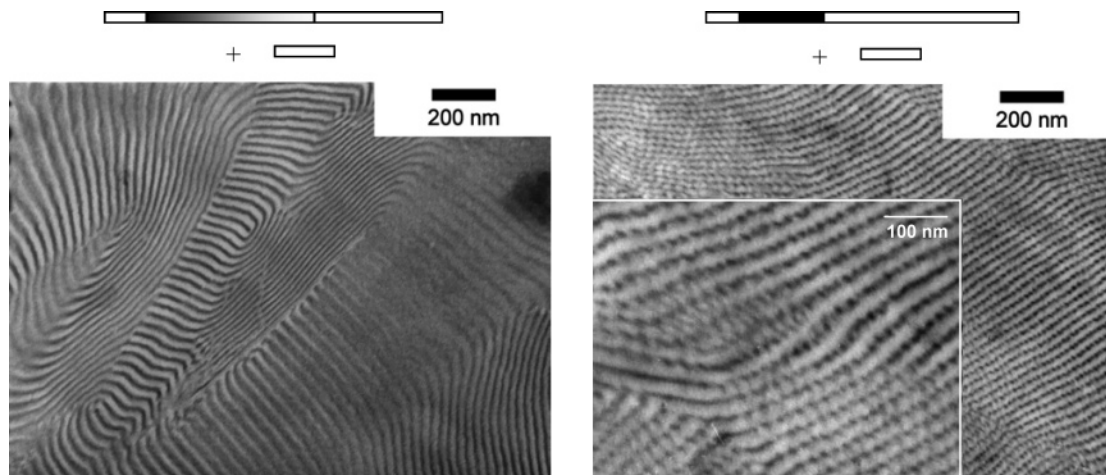


Figure 4. TEM micrographs of solvent cast and annealed blends of 15 wt % PS22 with (a) 85 wt % S1-G-S2 and (b) 85 wt % S1-B-S2.

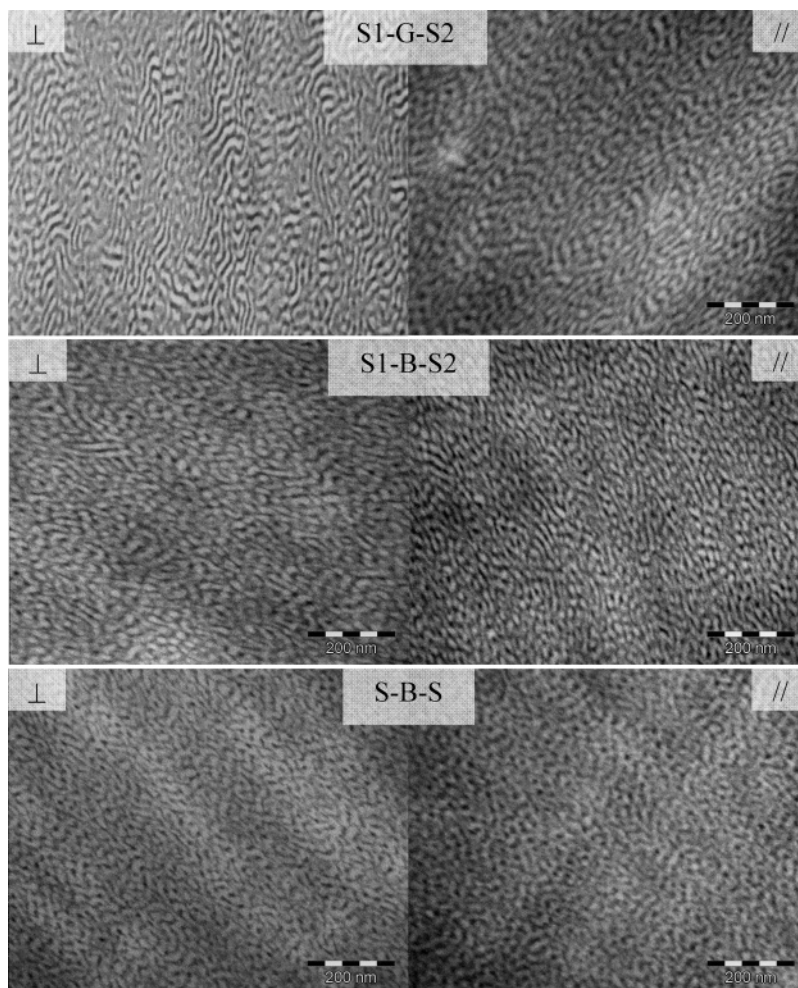


Figure 5. TEM micrographs of S1-G-S2, S1-B-S2 and S-B-S extruded from the melt at 180 °C. Sections cut perpendicular (left) and parallel (right) to the extrusion direction are shown.

were obtained on cross sections cut perpendicular to the extrusion direction, while the right ones were obtained on cross sections cut parallel to this direction. Both directions reveal roughly equivalent ill-defined cocontinuous morphologies reminiscent of quenched composition fluctuations. SAXS profiles of these extruded samples, shown in Figure 6, also suggest a poorly ordered yet microphase separated state. Compared to solvent cast films, first-order peaks are indeed broader, but at least one higher order reflection or a broad shoulder characteristic of liquid-like ordering is still visible. This result is

independent of shearing time, suggesting a stationary state within the extruder. The same morphologies are obtained independent of the initial block copolymer state. Both copolymer crumbs directly obtained from precipitation of the reaction mixture or highly ordered solvent cast films adopt the morphologies shown in Figure 5 after extrusion. The complex flow field which combines shearing and elongational forces apparently destroys the periodic lamellar or cylindrical arrangement of microdomains, and might even provoke their full dissolution within the extruder. Reversible shear-induced disordering of block

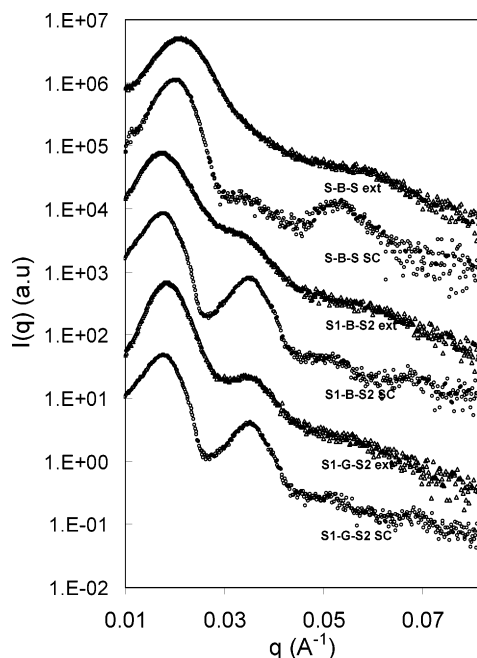


Figure 6. Room-temperature SAXS intensity profiles of solvent cast films (SC) and extruded strands (ext) of indicated copolymers.

copolymers has indeed been reported for certain types of multiblock copolymers and at high shear rates compatible with those developed during extrusion.^{59,60} Whether the poorly ordered morphologies of Figure 5 represent the actual copolymer state during extrusion or the early stages of microphase separation and morphology recovery upon exiting the die could not be verified in the context of this study. This would require in situ measurements of scattering profiles. The extruded strands are quenched in air and become rigid (below $T_{g,PS}$) in a few tens of seconds. Clearly, the periodic arrangement of microdomains does not have time to reconstruct in those short times. But it does so upon annealing the strands for a few hours at 180 °C, as illustrated in Figure 7 for S1-G-S2.

From a practical standpoint, the poorly ordered morphologies of Figure 5 and 7b are very important. Processing cycles of block copolymers for common film applications are indeed short and involve extrusion through a die followed by fast cooling. Actual morphologies used in these applications should more likely resemble those of Figure 5 than slow solvent cast morphologies. The low strain thermomechanical behavior of these extruded copolymers and its modeling are presented in the next section. A companion paper will focus on their high strain tensile properties, pure and blended with polystyrene.

III.4. Molecular and Mesoscopic Composition Profiles.

Linear dynamic mechanical behavior of the extruded copolymers was measured in tension as a function of temperature from -125 to +150 °C. The evolution of E' and $\tan \delta$ are plotted in Figure 8 for gradient and nongradient triblocks as well as the PS

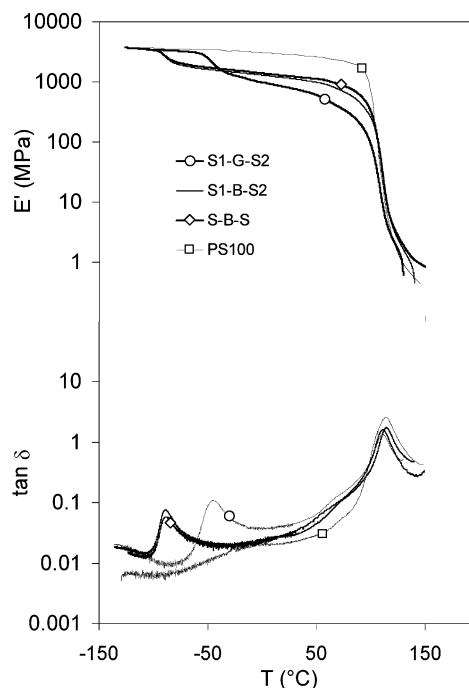


Figure 8. Dynamic storage modulus E' (top) and $\tan \delta$ (bottom) for indicated extruded and pressed copolymers and PS reference PS100.

reference PS100. All copolymers present a high- T_g microphase softening around $T_{g,hard} \sim 110$ °C, close to the pure PS reference. This confirms the hypothesis that hard microdomains contain pure PS blocks. The copolymers also present a second low- T_g microphase softening at a variable temperature $T_{g,soft}$ between -90 and -40 °C, depending on molecular structure. Based on the butadiene microstructure determined by 1H NMR, the theoretical T_g of pure butadiene microdomains calculated according to the Gordon-Taylor equation³⁶ lies around -90 °C.^{61,22} S-B-S and S1-B-S2, with low T_g 's of about -85 °C, should thus comprise almost pure butadiene microdomains. Gradient block copolymers have a higher $T_{g,soft}$ of about -40 °C. This indicates substantial mixing of S and B monomers in soft microdomains, consistent with previous results on similar copolymers.^{24,62} The progressive modulus drop between $T_{g,soft}$ and $T_{g,hard}$ indicates softening of interfacial material which, as expected, is more important for S1-G-S2. Despite their different molecular architectures, S1-B-S2 and S-B-S present very similar evolutions of modulus and $\tan \delta$. The only noticeable difference is the earlier onset of modulus drop for S1-B-S2 when approaching $T_{g,PS}$. This might be related to the lower temperature motion of short S1 blocks in the asymmetric copolymer. It is important to note that similar evolutions of modulus and the same soft and hard microphases were recorded for solvent cast films, but with more pronounced modulus drops at $T_{g,soft}$ for the two lamellar copolymers. Long-range order would thus be most affected by extrusion followed by rapid cooling,

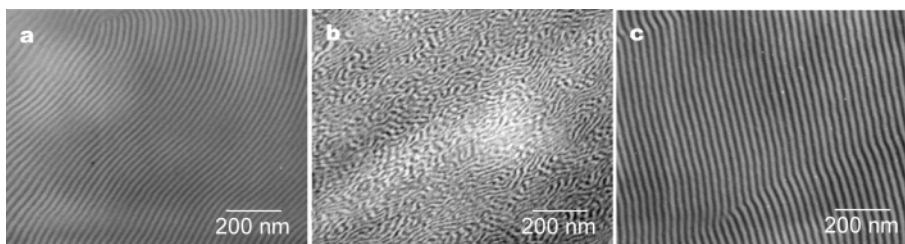


Figure 7. Self-assembly of S1-G-S2 (a) solvent cast and annealed, (b) extruded at 180 °C and air cooled, and (c) annealed at 180 °C for 48 h after extrusion.

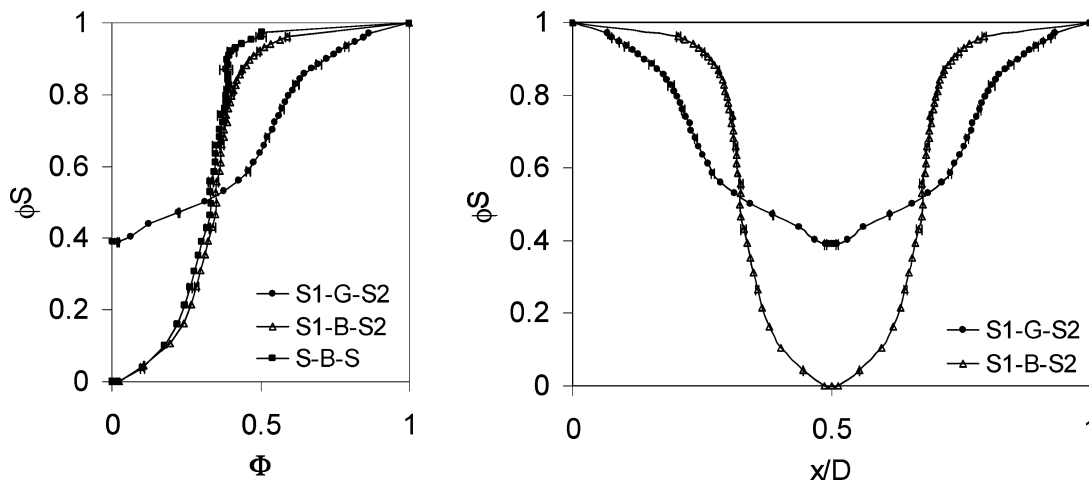


Figure 9. (a) Local styrene volume fraction ϕ_S as a function of cumulative soft phase fraction Φ determined from at least two independent DMA experiments for indicated copolymers. (b) Local styrene volume fraction as a function of normalized distance across one lamellar period D for S1-G-S2 and S1-B-S2 assuming a local planar geometry of the interface.

while the nature itself of microdomains and interfaces is only slightly altered. In the following analysis, only extruded samples are considered.

Modeling dynamic modulus data with an appropriate composite equation can be used to quantify volume fractions and composition of soft and hard microphases and interfaces in these copolymers.^{15,25} The copolymer modulus at a given temperature is indeed related to the volume fraction of soft (mobile) copolymer blocks at this temperature. This ratio is further affected by the geometry and size of soft microdomains and their orientation with respect to the external applied stress. Several models try to quantify this link between modulus and dispersions of soft inclusions of a given geometry. The simplest is the Kerner model which considers spherical dispersions of noninteracting soft inclusions in a hard matrix. Isotropic in nature, it does not apply to lamellar or cylindrical block copolymers, for which more complex expressions have been used.²⁴ Extruded samples, which present a nearly isotropic distribution of soft and hard microdomains lacking long-range order, might follow this expression.

To model the temperature dependence of their elastic modulus, these copolymers were thus considered to be composed of rubbery spherical cores softening at a temperature T_{gsoft} surrounded by interfacial shells with a gradient composition richer in PS as it is farther from the core and softening over a range of temperatures. These are dispersed in a hard matrix softening at T_{ghard} . At each temperature between T_{gsoft} and T_{ghard} , a portion of the interface becomes mobile, consequently increasing the volume fraction of soft phase. Assuming that the softened phase ($T_{\text{g}} < T$) has a single modulus E_d , and that the hard phase ($T_{\text{g}} > T$) has a single modulus E_m , it is possible to calculate the fraction of softened material at each temperature using the Kerner model. This model assumes that there is good adhesion between particles and matrix and that Poisson's ratio ν_c of the composite material (here the copolymer) is equal to that of the matrix material ν_m . The elastic modulus of the copolymer E_c is then given by

$$\frac{E_c}{E_m} = \frac{(1 - \Phi)E_m + \beta(\alpha + \Phi)E_d}{(1 + \alpha\Phi)E_m + \alpha\beta(1 - \Phi)E_d} \quad (13)$$

where E_m is the matrix (PS) modulus, Φ is the volume fraction of soft phase, E_d its modulus and $\alpha = (2(4 - 5\nu_m))/((7 - 5\nu_m))$ and $\beta = ((1 + \nu_m))/((1 + \nu_d))$, ν_d being Poisson's ratio of the rubbery dispersed phase. Provided the dispersed phase is a soft

polymer with a small E_d compared to E_m , eq 13 simplifies to

$$E_c = \frac{(1 - \Phi)}{(1 + \alpha\Phi)} \times E_m \quad (14)$$

This form of Kerner's model was used to relate the copolymer mechanical properties to the volume fraction of soft inclusions at each temperature according to

$$\Phi = \frac{E_m - E_c}{E_m + \alpha E_c} \quad (15)$$

where E_c and E_m are given the experimentally measured copolymer and pure PS moduli values, respectively. Each incremental shell softening between T and $T + \Delta T$, with volume $\Delta\Phi(T) = \Phi(T + \Delta T) - \Phi(T)$, is a mixture of S and B monomers with theoretical T_{g} equal to T . The local weight fraction of styrene $w_S(T)$ of this shell can be evaluated according to the Gordon-Taylor equation:³⁶

$$w_S(T) = \frac{T - T_{\text{gPB}}}{K(T_{\text{gPS}} - T) + (T - T_{\text{gPB}})} \quad (16)$$

where T_{gPS} and T_{gPB} are glass transitions of pure PS and PB, respectively, $K = \Delta\beta_{\text{PS}}/\Delta\beta_{\text{PB}}$, and $\Delta\beta_{\text{PS}}$ and $\Delta\beta_{\text{PB}}$ are the differences in thermal expansion between the glassy and liquid states of PS and PB respectively.⁶¹ This composition is then converted to a local PS volume fraction $\phi_S(T)$ using density data.⁶¹ This analysis has a physical meaning as long as $\Delta\Phi(T)$ is greater or equal to zero. Since negative values were often obtained above 95 °C, this was set as the highest temperature at which the model could be applied. Beyond 95 °C, ϕ_S and Φ were set to one since it corresponds to the onset of the glass transition of pure PS.

Plotting $\phi_S(T)$ as a function of cumulative $\Phi(T)$ then yields volumetric composition profiles across microdomains which are shown in Figure 9a for each copolymer. These are average profiles obtained from at least two independent DMA experiments for each copolymer. The resulting standard deviation on $\Phi(T)$ is plotted every four data points. These profiles give the evolution of local styrene volume fraction when traveling from the heart of a soft microdomain to the matrix. They nicely illustrate the effect of a gradient middle block on soft phase and interfaces in these copolymers. First, they confirm that self-assembled gradient copolymers do not contain pure B micro-

domains but soft microdomains mixed with S. The soft phase of S1-G-S2 contains as much as 40 vol % S, and therefore occupies a much higher fraction of the material. Pure PS microdomains are consequently smaller. The progression from butadiene-rich to styrene-rich compositions is also very smooth and gradual compared to the blocky analogues S1-B-S2 and S-B-S, revealing broad interfaces. On the other hand, S1-B-S2 and S-B-S present almost identical sharp interfacial profiles, as expected from their similar evolutions of modulus (Figure 8). As discussed earlier, the main and reproducible difference occurs prior to T_{gps} , where short S1 blocks localized close to the interface tend to smooth the interfacial profile.

Provided a very local lamellar arrangement (local planar geometry of the interface) can still be assumed for S1-G-S2 and S1-B-S2 after extrusion, the cumulative volume fraction of soft phase $\Phi(T)$ of Figure 9a is equivalent to the normalized distance from the center of a soft microdomain to the center of the adjacent hard microdomain (half a microdomain period). The y -axis still gives the local volume fraction of styrene at each position. Combining two of these profiles yields the mesoscopic composition profiles across one lamellar period D shown in Figure 9b for S1-G-S2 and S1-B-S2. Compared to its nongradient analogue, the gradient copolymer displays a smooth composition profile with broad interfaces reminiscent of weakly segregated block copolymers. Soft (B-rich) microdomains also occupy a higher fraction of the material.

The validity of the present analysis and the composition profiles of Figure 9 can be tested by calculating the global styrene fraction they predict according to

$$\Phi_S = \sum \phi_{S,i} \Delta\Phi_i + (1 - \Phi_{95}) \quad (17)$$

where each volume increment $\Delta\Phi_i$ is multiplied by its local styrene content $\phi_{S,i}$ and summed over all temperatures up to 95 °C. The remaining pure styrene fraction softening at T_{gps} is $(1 - \Phi_{95})$. Equation 17 yields 70, 66, and 71 vol % S for S1-G-S2, S1-B-S2, and S-B-S, respectively. These are in reasonable agreement with the ^1H NMR compositions listed in Table 1. The volume fraction of soft microdomains at room temperature can also be estimated from the Φ -axis value at $\phi_S = 0.78$ ($T = 25$ °C) in Figure 9a. S1-G-S2, S1-B-S2 and S-B-S would then contain 58, 40, and 38 vol % soft phase, respectively, at this arbitrary temperature. From a mechanical standpoint, the present analysis gives direct evidence for the role of gradient sections in these rubbery/glassy block copolymers: they offer a way to maximize the soft phase volume fraction at a given temperature while keeping the diene content low. The higher the concentration of polar modifier initially added in the reaction mixture, the broader and smoother the gradient composition profile will be, and so will be the mesoscopic composition profile across microdomains. These will in turn determine the mechanical properties of these gradient triblock copolymers and their blends with polystyrene. The present combined use of Kerner model and the Gordon-Taylor expression provides a very simple way to quantify the effect of molecular structure on soft, hard, and interfacial material in these self-assembled copolymers. However, it is important to note that this analysis and quantitative comparison of the different copolymers was only possible because extrusion produces roughly identical isotropic microphases for all copolymers. For solvent cast films with large grains of anisotropic morphologies, a more complex expression than the Kerner model would have had to be considered.

IV. Conclusions

Asymmetric gradient triblock copolymers of butadiene and styrene, denoted S1-G-S2, were prepared by a two-step anionic copolymerization in cyclohexane in presence of THF. After homopolymerization of S1, a copolymerization (second) step yields a strong gradient originally rich in B and terminated by a pure block S2. The asymmetry between S1 and S2 and the gradient composition profiles were quantified by modeling conversion data with a Markov model. Equilibrium self-assembly is strongly affected by this particular molecular structure. Asymmetry is responsible for a shift of the phase diagram toward PS-rich compositions, in agreement with theory. Hence, lamellae form at 70 vol % PS, instead of cylinders. Modeling of SAXS lamellar periods suggests that this lamellar phase is not accompanied by substantial pull out of short S1 blocks into B microdomains. Instead, S1 blocks more likely self-assemble in a bidisperse brush with S2 blocks, and bridging configuration of the triblock should thus be possible. The molecular origin of the lamellar phases of these asymmetric triblocks is then essentially similar to the co-surfactant effect in binary blends of diblock copolymers with short and long A blocks. The gradient middle block further shifts morphology boundaries toward S-rich compositions by swelling B microdomains with statistical styrene units incorporated during copolymerization. Highly robust lamellae thus form at 70 vol % S.

The strong elongational and shear flow fields developed during extrusion destroy this equilibrium self-assembly. After melt processing, gradient triblocks and their blocky analogues all present poorly ordered isotropic morphologies. Yet, the nature of the microphases and interface detected by DMA is hardly changed. All copolymers present a pure PS microphase and a soft microphase with variable T_g . A simple method based on the Kerner model combined with the Gordon-Taylor equation was used to describe dynamic tensile moduli of these extruded copolymers. This analysis yields the volume fraction of soft phase and its styrene content as a function of temperature. Mesoscopic composition profiles across microdomains could then be built, which clearly demonstrate the role of the gradient on the interface and soft microdomain volume fractions. Gradient triblock copolymers display smooth composition profiles with broad interfaces compared to their blocky analogues. Their soft phase, which is a mixture of S and B, accounts for as much as 50 vol % of the material despite a global styrene volume fraction of 70%. This will have important consequences on the high-strain tensile properties of these copolymers and their blends with PS.

Acknowledgment. We thank C. Degoulet and M. Millequant for their help with SEC analyses and V. Loustalot for the pilot-scale anionic syntheses. We are also deeply indebted to our colleagues from Total-Petrochemicals, in particular B. Vuillemin who initiated this project, and J. Neelen for helpful discussions. The authors thank the ARKEMA-CERDATO LEM laboratory for facilitating X-ray scattering experiments and, in particular, S. Lebreton and the UPR-5-ESPCI-CNRS TEM group for technical help. This work further benefited from stimulating discussions with M. Cloître and F. Tournilhac. We acknowledge financial support from CNRS, ESPCI, and TOTAL.

References and Notes

- (1) Lodge, T. P. *Macromol. Chem. Phys.* **2003**, *204*, 265.
- (2) Ruzette, A.-V.; Leibler, L. *Nat. Mater.* **2005**, *4*, 19. Leibler, L. *Prog. Polym. Sci.* **2005**, *30*, 898.

- (3) Bates, F. S.; Fredrickson, G. H. *Annu. Rev. Phys. Chem.* **1991**, *41*, 525.
- (4) Leibler, L. *Macromolecules* **1980**, *13*, 1602.
- (5) Mayes, A. M.; de la Cruz, M. O. *J. Chem. Phys.* **1989**, *91*, 7228; *J. Phys. Chem.* **1991**, *95*, 4670.
- (6) Dobrynin, A. V.; Erukhimovitch, I. Y. *Macromolecules* **1993**, *26*, 276.
- (7) Milner, S. T. *Macromolecules* **1994**, *27*, 2333.
- (8) Hadjichristidis, N.; Lohse, D. J. *Curr. Opin. Colloid Interface Sci.* **1997**, *2*, 171 and references therein.
- (9) Matsen, M. W.; Thompson, R. B. *J. Chem. Phys.* **1999**, *111*, 7139.
- (10) Matsen, M. W. *J. Chem. Phys.* **2000**, *113*, 5539.
- (11) Pakula, T.; Matyjaszewski, K. *Macromol. Theory Simul.* **1996**, *5*, 987.
- (12) Knoll, K.; Niessner, N. *Macromol. Symp.* **1998**, *132*, 231 and references therein.
- (13) Priddy, D. In *Encyclopedia of Polymer Science and Technology*; John Wiley & Sons: New York; 2006; Vol. 4, p 252.
- (14) LeKhac, B. *Abstr. Pap. Am. Chem. Soc.* **1989**, *197*, 137.
- (15) Tsukahara, Y.; Nakamura, N.; Hashimoto, T.; Kawai, H. *Polym. J.* **1980**, *12*, 455.
- (16) Kryszewski, M. *Polym. Adv. Tech.* **1998**, *9*, 244.
- (17) Matyjaszewski, K.; Ziegler, M. J.; Arehart, S. V.; Gresztal D.; Pakula, T. *J. Phys. Org. Chem.* **2000**, *13*, 775.
- (18) Min, K.; Li, M.; Matyjaszewski, K. *J. Polym. Sci., Part A: Polym. Chem.* **2005**, *43*, 3616.
- (19) Aksimentiev, A.; Holyst, R. *J. Chem. Phys.* **1999**, *111*, 2329.
- (20) Kuchanov, S.; Kok, C.; ten Brinke, G. *Macromolecules* **2002**, *35*, 7804.
- (21) Lefebvre, M. D.; de la Cruz, M. O.; Shull, K. R. *Macromolecules* **2004**, *37*, 1118.
- (22) Kraus, G.; Childers, C. W.; Gruver, J. T. *J. Appl. Polym. Sci.* **1967**, *11*, 1581.
- (23) Kraus, G.; Rollmann, K. W. *Angew. Makromol. Chem.* **1971**, *16/17*, 271.
- (24) Hashimoto, T.; Tsukahara, Y.; Tachi, K.; Kawai, H. *Macromolecules* **1983**, *16*, 648.
- (25) Annighöfer, F.; Gronski, W. *Colloid Polym. Sci.* **1983**, *261*, 15. Gronski, W.; Annighöfer, F.; Stadler, R. *Makromol. Chem.* **1984**, *6*, 141.
- (26) Samseth, J.; Spontak, R. J.; Smith, S. D.; Ashraf, A.; Mortensen, K. *J. Phys. IV* **1993**, *3*, 59.
- (27) Zielinski, J. M.; Spontak, R. J. *Macromolecules* **1992**, *25*, 5957. Kane, L.; Spontak, R. J. *Macromolecules* **1994**, *27*, 1267.
- (28) Laurer, J. H.; Smith, S. D.; Samseth, J.; Mortensen, K.; Spontak, R. J. *Macromolecules* **1998**, *31*, 4975. Laurer, J. H.; Fung, J. C.; Sedat, J. W.; Smith, S. D.; Samseth, J.; Mortensen, K.; Agard, D. A.; Spontak, R. J. *Langmuir* **1997**, *13*, 2177.
- (29) Hodrokoukes, P.; Floudas, G.; Pispas, S.; Hadjichristidis, N. *Macromolecules* **2001**, *34*, 650.
- (30) Adhikari, R.; Michler, G. H. *Prog. Polym. Sci.* **2004**, *29*, 949.
- (31) Adhikari, R.; Godehardt, R.; Lebek, W.; Weidisch, R.; Michler, G. H.; Knoll, K. *J. Macromol. Sci. Phys.* **2001**, *40*, 833.
- (32) Adhikari, R.; Michler, G. H.; Lebek, W.; Goerlitz, S.; Weidisch, R.; Knoll, K. *J. Appl. Polym. Sci.* **2002**, *85*, 701.
- (33) Flory, P. J. *Principles of Polymer Chemistry*; Cornell University Press: Ithaca: NY, 1953; Chapter 5.
- (34) Odian, G. *Principles of Polymerization*, 3rd ed.; John Wiley and Sons, Inc.: New York; 1991; Chapter 6.
- (35) Kerner, E. H. *Proc. Phys. Soc. London, Sect. B* **1956**, *69*, 808.
- (36) Gordon, M.; Taylor, J. S. *J. Appl. Chem.* **1952**, *2*, 493.
- (37) Kraus, G.; Stacy, C. J. *J. Polym. Sci., Part A-2: Polym. Phys.* **1972**, *10*, 657.
- (38) Mochel, V. D. *Macromolecules* **1969**, *2*, 537.
- (39) Grimaldi, S.; Finet, J.-P.; Le Moigne, F.; Zeghdaoui, A.; Tordo, P.; Benoit, D.; Fontanille, M.; Gnanou, Y. *Macromolecules* **2000**, *33*, 1141.
- (40) Ruzette, A.-V.; Tencé-Girault, S.; Leibler, L.; Chauvin, F.; Bertin, D.; Guerret, O.; Gérard, P. *Macromolecules* **2006**, *39*, 5804.
- (41) Zelinski, R.; Childers, C. W. *Rubber Chem. Technol.* **1968**, *41*, 161.
- (42) Hsieh, H. L. In *Block and Graft Copolymers*; Burke, J. J., Weiss, V., Eds.; Syracuse University Press: Syracuse, NY; 1973.
- (43) Johnson, A. F.; Worsfold, D. J. *Makromol. Chem.* **1965**, *85*, 273.
- (44) Van Beylen, M.; Bywater, S.; Smets, G.; Szwarc, M.; Worsfold, D. J. *Adv. Polym. Sci.* **1988**, *86*, 87 and references therein.
- (45) Young, R. N.; Quirk, R. P.; Fetters, L. J. *Adv. Polym. Sci.* **1984**, *56*, 1 and references therein.
- (46) Ohlinger, R.; Bandermann, F. *Makromol. Chem. Macromol. Chem. Phys.* **1980**, *181*, 1935.
- (47) Kok, C. On the Phase Behavior of Polydisperse Copolymers: (tapering, oscillations and destruction). Thesis dissertation, University of Groningen, 2001.
- (48) Sakurai, S.; Mori, K.; Okawara, A.; Kimishima, K.; Hashimoto, T. *Macromolecules* **1992**, *25*, 2679.
- (49) Roe, R.-J.; Zin, W. C. *Macromolecules* **1980**, *13*, 1221.
- (50) Semenov, A. N. *Sov. Phys. JETP* **1985**, *61*, 733.
- (51) Kurata, M.; Tsunashima, Y. In *Polymer Handbook*, 4th ed.; Brandrup, J., Immergut, E. H., Grulke, E. A., Eds.; John Wiley and Sons: New York; 1999; Chapter 7; p 47.
- (52) Birshtein, T. M.; Liatskaya, Y. V.; Zhulina, E. B. *Polymer* **1990**, *31*, 2185. Zhulina, E. B.; Birshtein, T. M. *Polymer* **1991**, *32*, 1299.
- (53) Shi, A. C.; Noolandi, J. *Macromolecules* **1994**, *27*, 2936. Shi, A. C.; Noolandi, J.; Hoffmann, H. *Macromolecules* **1994**, *27*, 6661.
- (54) Hashimoto, T.; Yamaguchi, D.; Court, F. *Macromol. Symp.* **2003**, *195*, 191. Yamaguchi, D.; Hashimoto, T. *Macromolecules* **2001**, *34*, 6495 and references therein.
- (55) Court, F.; Hashimoto, T. *Macromolecules* **2001**, *34*, 2536. Court, F.; Hashimoto, T. *Macromolecules* **2002**, *35*, 2566.
- (56) Hajduk, D. A.; Takenouchi, H.; Hillmyer, M. A.; Bates, F. S.; Vigild, M. E.; Almdal, K. *Macromolecules* **1997**, *30*, 3788.
- (57) Yang, L.; Gido, S. P.; Mays, J. W.; Pispas, S.; Hadjichristidis, N. *Macromolecules* **2001**, *34*, 4235.
- (58) Adhikari, R.; Huy, T. A.; Buschnakowski, M.; Michler, G.H.; Knoll, K. *New J. Phys.* **2004**, *6*, 28.
- (59) Tepe, T.; Hajduk, D. A.; Hillmyer, M. A.; Weimann, P. A.; Tirrell, M.; Bates, F. S.; Almdal, K.; Mortensen, K. *J. Rheol.* **1997**, *41*, 1147. Hajduk, D. A.; Tepe, T.; Takenouchi, H.; Tirrell, M.; Bates, F. S.; Almdal, K.; Mortensen, K. *J. Chem. Phys.* **1998**, *108*, 326.
- (60) Vigild, M. E.; Sugiyama, M.; Chaffin, K. A.; Bates, F. S. *Macromolecules* **2001**, *34*, 951.
- (61) Brandrup, J.; Immergut, E. H.; Grulke, E. A. *Polymer Handbook*, 4th Ed.; John Wiley and Sons: New York; 1999.
- (62) Huy, T. A.; Hai, Hong Hai, L.; Adhikari, R.; Weidisch, R.; Michler, G. H.; Knoll, K. *Polymer* **2003**, *44*, 1237.

MA062723U